frontiers | Frontiers in Energy Research

TYPE Original Research
PUBLISHED 14 September 2023
DOI 10.3389/fenrg.2023.1277648

OPEN ACCESS

EDITED BY
Peng Tan,
CNPC Engineering Technology R&D Company Limited, China

REVIEWED BY
Yan Xi,
Beijing University of Technology, China
Chao Wang,
Yangtze University, China

*CORRESPONDENCE
Jiangshuai Wang,
wjs125126@163.com

RECEIVED 15 August 2023
ACCEPTED 04 September 2023
PUBLISHED 14 September 2023

CITATION
Xuan L and Wang J (2023), A new type of high hardness coating for improving drill bit stability in unconventional oil and gas development.
Front. Energy Res. 11:1277648.
doi: 10.3389/fenrg.2023.1277648

A new type of high hardness coating for improving drill bit stability in unconventional oil and gas development

Lingchao Xuan[1,2] and Jiangshuai Wang[1,3]*

[1]State Key Laboratory of Shale Oil and Gas Enrichment Mechanisms and Effective Development, Beijing, China, [2]Sinopec Research Institute of Petroleum Engineering Co. Ltd., Beijing, China, [3]School of Petroleum and Gas Engineering, Changzhou University, Changzhou, China

In deep unconventional oil and gas development, the problem faced is that PDC bits are eroded by solid-liquid high-speed fluids, resulting in damage. It has led to serious damage to the stability of the drill bit, a decrease in the service life of the drill bit, and an increase in the difficulty in efficient drilling. The essence is that the surface hardness and erosion resistance of the drill bit are not strong enough. Therefore, improving the stability of drill bits is a crucial and urgent problem to be solved. In this paper, Ni60A + 20% WC + 0.3% graphene composite coatings were prepared on a Q235 steel substrate, which is a new type of high hardness coating. Moreover, the effects of microstructure and microhardness of the composite coatings at different laser powers (800 W, 1200 W, 1600 W, and 2000 W) were investigated. The results show that the laser power can significantly affect the microstructure of the coating. The phase composition of the composite coatings is essentially the same at different laser powers. However, there are significant differences in the content of each phase. When the laser power is higher than 1200W, the content of $M_{23}C_6$, Cr_3C_2 and Fe_3C in the composite coating increases and the microhardness of the coating decreases. When the laser power is below 1200 W, the dilution rate of the substrate is low and a metallurgical bond cannot be formed between the composite coating and the substrate.

KEYWORDS

laser cladding, laser power, WC particles, Ni-based alloys, drill bit

1 Introduction

During the unconventional oil and gas high-speed well construction process (Tan et al., 2020; Wang et al., 2021), the stability of the drill bit is severely damaged, and the service life of the drill bit decreases (Dontsov, 2022; Wang et al., 2023a; Huang et al., 2023). Improving the stability of drill bits is a crucial and urgent issue to be addressed, especially in the development process of unconventional oil and gas resources such as deep shale oil and gas (Tan et al., 2021; Ma et al., 2022; Wang et al., 2023b). It is related to drilling speed, development efficiency, and national energy security issues. Laser cladding technology uses a high-energy laser beam to rapidly heat and cool a material surface for the preparation of protective coatings with properties such as high hardness, wear and corrosion resistance (Wang et al., 2022a; Chen et al., 2023; Wu et al., 2023). The protective coatings prepared by laser cladding technology are able to achieve metallurgical bonding with the metal substrate (Qunshuang et al., 2016). Furthermore, the coatings are characterized by a homogeneous microstructure, fine grain size and low dilution rates (Meng et al., 2022; Xu et al., 2022; Ren

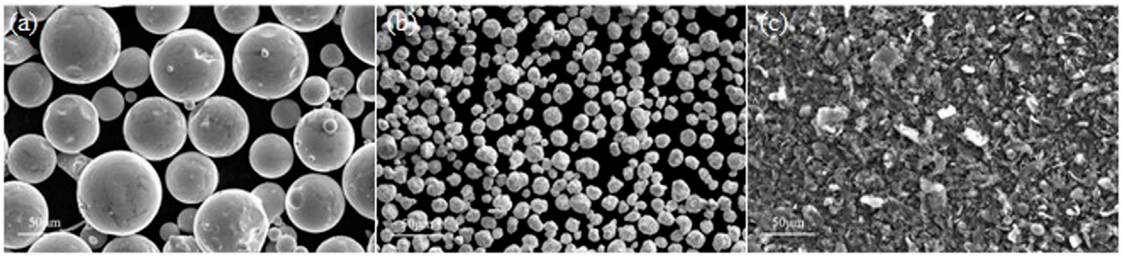

FIGURE 1
The SEM of the powder; **(A)** Ni60, **(B)** WC, **(C)** Graphene.

et al., 2023). The coatings prepared by laser cladding technology have excellent microstructural properties and mechanical properties. Moreover, these have received widespread attention in the fields of aerospace, industrial machinery, oil and gas chemicals (Jie et al., 2022; Kendall et al., 2023). Nickel-based alloy coatings are widely used for laser cladding due to their affordability and good self-lubricating properties and corrosion resistance (Zhang et al., 2023a; Li et al., 2023). Ceramic-based particles such as WC, TiC and SiC are often added to nickel-based alloy coatings as an additive phase to improve the mechanical properties of the coating (Hu et al., 2022; Chen et al., 2022; Wu et al., 2022; Zhang et al., 2023b).

Nickel-based alloy/WC coatings have been studied by a large number of academics for their excellent corrosion and wear resistance properties. Hu et al. (Hu et al., 2022b) found that grain refinement in the new WC coating increased with increasing WC content. In the process, the thermomechanical stability and hardness of the coating also increased. Li et al. (2022) found that the WC content in Ni60/WC coatings can influence the microstructure and phase components of the coatings. In detail, the WC content is positively correlated with the hardness and wear resistance of the coatings. Yao et al. (2018) found that the distribution of WC in Ni60/WC coatings can affect the mechanical properties of the coatings. And, the denser the WC is on the surface of the coating. There are the better the hardness and wear resistance of the coating. Wu et al. (2004) found that lower laser power would result in the deposition of WC towards the bottom of the coating. In addition, the interface between the Ni-based alloy and the WC particles would be the initiation point for cracks within the coating. Xu et al. (2014) found that the appearance of cracks in Ni-based alloy/WC coatings was related to the WC distribution. Chiang and Chen (2007) found that increasing the laser power facilitated WC decomposition and reduced the WC content in the coating. Wang et al. (2022b) and Wu et al. (2004) found that the preparation of gradient Ni-based alloy-WC coatings on the substrate surface was able to reduce the tendency of the coatings to crack. Due to its excellent toughness and self-lubricating properties, Xia et al. (2022) and Chang et al. (2023) found that the addition of graphene into metal matrix composite coatings, was beneficial in reducing the tendency of the coatings to crack. Therefore, appropriate melting power, WC content or the introduction of graphene are beneficial in reducing the cracking tendency of Ni-based alloy/WC coatings.

In the present work, graphene/Ni60/WC coatings were prepared on the surface of Q235 steel using pre-powdered laser melting. The effect of laser melting power on the microstructure, composition and coating hardness of the coatings was investigated.

TABLE 1 Chemical compositions of Q235 and Ni60A powder (wt.%).

	Fe	C	Si	Mn	Cr	Ni	Cu	O
Q235	Bal.	0.16	0.26	0.15	0.02	0.025	0.024	-
Ni60A	4.63	0.76	4.11	-	16.58	Bal.	-	0.03

2 Materials and experimental process

2.1 Material and sample preparation

The substrate material used for the laser cladding experiments was Q235 steel with a specimen size of 100 mm × 100 mm × 5 mm. The powder material used for laser cladding is a mixture of Ni60A + 20% WC + 0.3% graphene. The particle size range of Ni60A powder is 50 μm–150 μm and its microscopic morphology is shown in Figure 1A. The composition of Q235 steel and Ni60A powder are shown in Table 1. The WC powder particle size ranges from 15 μm to 45 μm and its microscopic morphology is shown in Figure 1B. The graphene is multilayer graphene and its microscopic morphology is shown in Figure 1C.

Sodium dodecylbenzene sulfonate was mixed with graphene in a ratio of 1:10. After adding an appropriate amount of alcohol, the dispersion of graphene was carried out using an ultrasonic shaker, followed by drying using a vacuum drying oven. The treated graphene, WC powder and Ni60A powder were proportionally configured to produce a Ni60A + 20% WC+0.3% graphene blend. The powder is dried for 2 h and then blended for 8 h using a planetary ball mill (DECO, type PBM-AD-4L) set at 300 r/min autogenous and 4 r/min metric.

The Q235 steel substrate is sanded with 60 grit sandpaper before the start of the pre-powdering process. Polyvinyl cellulose was used to prepare a polyvinyl alcohol solution (ratio 8:1000), which was mixed with Ni60A + 20% WC + 0.3% graphene mixed powder. The mixed powder is spread on the surface of the specimen to a thickness of 1.5 mm and the work is carried out using a laser cladding processing system. The laser cladding power was selected as 800 W, 1,200 W, 1,600 W, and 2,000 W respectively, with the remaining parameters shown in Table 2.

TABLE 2 Ni60A + 20% WC + 0.3% graphene mixed powder laser cladding process parameters.

Coatings	DepositedSpeed (m/min)	Overlapping ratio (%)	Spot diameter (g/min)	Shielding gas flow (L/min)
	0.35	50%	14.8	15

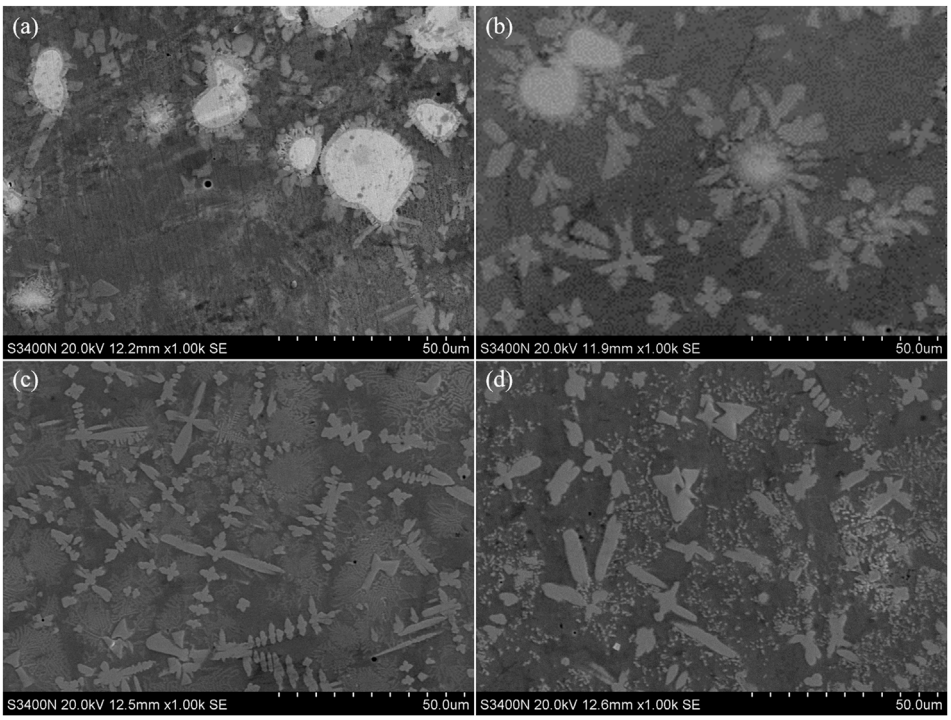

FIGURE 2
Cross-sectional morphology of the top of a Ni60A + 20% WC + 0.3% graphene composite coating by laser cladding at different laser powers: **(A)** 800 W, **(B)** 1,200 W, **(C)** 1,600 W, **(D)** 2,000 W.

2.2 Analysis methods

The morphology and elemental distribution of the cross-sections were analyzed at different locations using a Hitachi S-3400 N scanning electron microscope (SEM) and an energy spectrometer (EDS). X-ray diffraction (XRD) using a Bruker D8 X-ray diffractometer goniometer, Cu target K_α rays, voltage 40 kV, current 30 mA, diffraction angle 10°–90° scan speed 6°/min. The microhardness of the clad surface was tested using a micro-vickers hardness tester (HVS-1000A) with an applied load of 0.2 kg and a holding time of 15 s. The hardness was measured using a four-point measurement method.

3 Results and discussion

3.1 Cross-sectional morphological analysis

Figure 2 shows the cross-sectional morphology of the top of a Ni60A + 20% WC + 0.3% graphene composite coating by laser cladding at different laser powers. There are significant differences in the microstructure of the top part of the coating at different laser powers. At a laser power of 800 W, a large number of WC particles were present in the top part of the coating and decarburized at high temperatures to form W_2C, W atoms and C atoms (Liao et al., 2023). The W and C atoms expanded into the Ni-based alloy and reacted with it. New phases in the form of blocks and rods are formed around the WC particles. At 1,200 W, the decomposition of the WC particles is promoted by the increased heat input. The size of the WC particles in the top part of the coating decreases significantly and the precipitated phase is predominantly rod and snowflake shaped. When the laser power was 1,600 W, no WC particles were observed in the top part of the coating. It indicates that the WC particles had completely decomposed and that the precipitated phase in the top part of the coating was mainly in the form of flocculent and fishbone structures. This is due to the further elevation of the heat input promoting the dissolution of W and C atoms into the Ni-based alloy. In addition, small porous defects appear in the top part of the coating.

To further characterize the distribution of elements in the characteristic areas of the coating, a surface scan analysis was carried out on the top area of the coating with a laser power of 1,200 W. As shown in Figure 3, W and Si elements are enriched in WC particles and in the precipitation phase of rod and snowflake structures. There is a significant enrichment of Cr elements around the WC particles, and it can be assumed that the C atoms from the WC decomposition reacted with the Cr in the Ni-based alloy. The

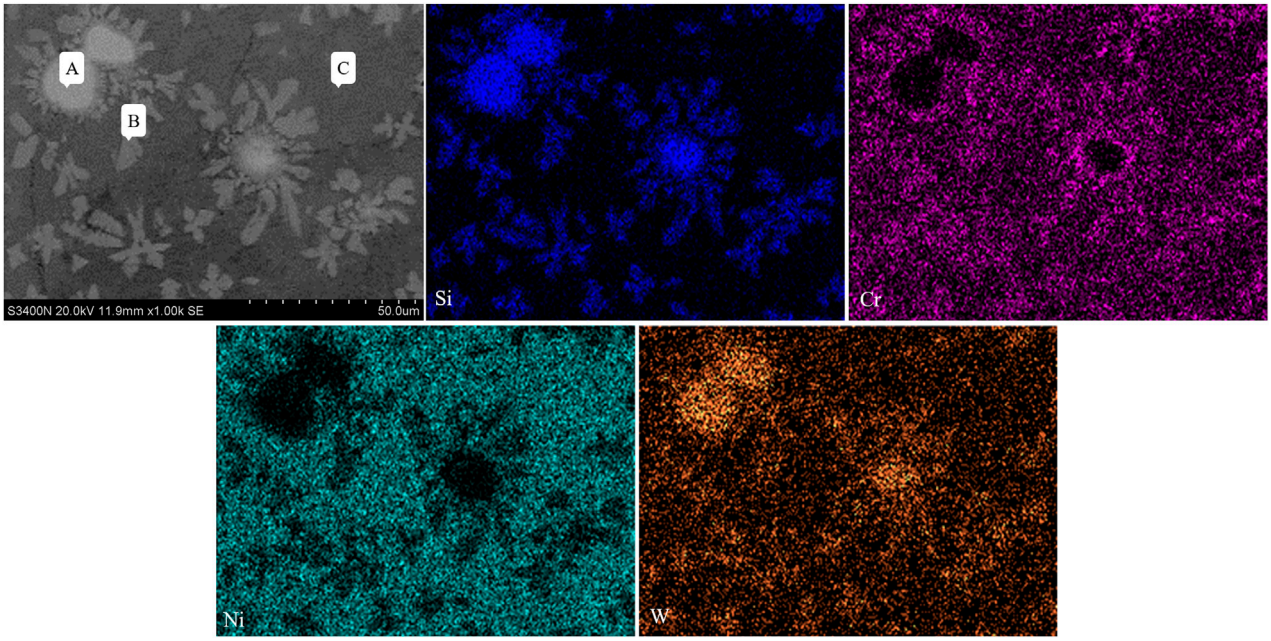

FIGURE 3
EDS map scanning results of the coating at a laser power of 1,200 W.

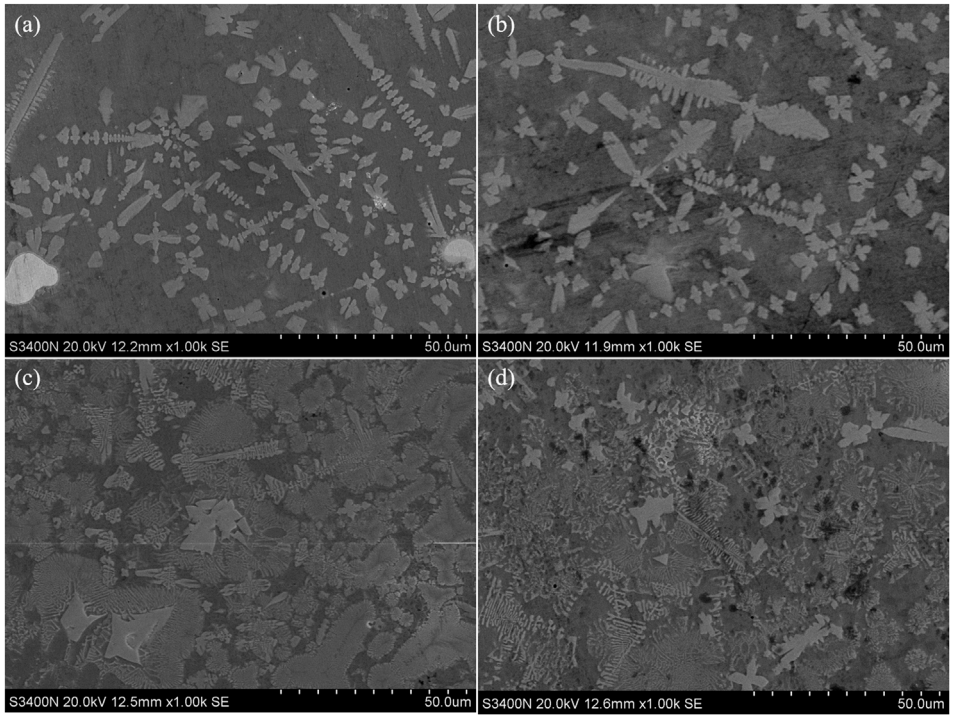

FIGURE 4
Cross-sectional morphology of the middle of a Ni60A + 20% WC + 0.3% graphene composite coating by laser cladding at different laser powers: **(A)** 800 W, **(B)** 1,200 W, **(C)** 1,600 W, **(D)** 2,000 W.

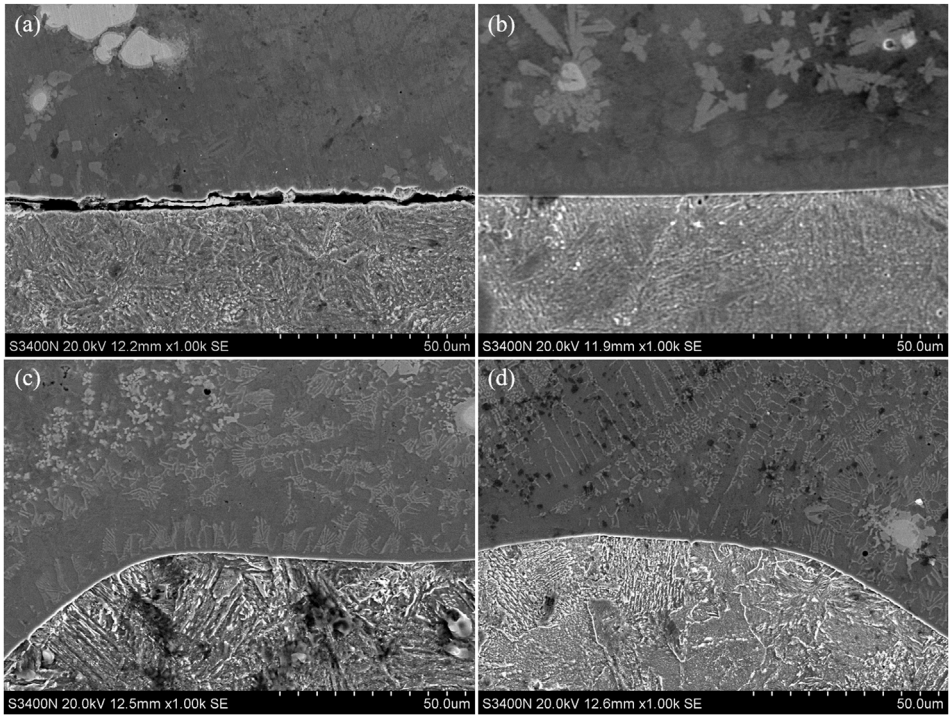

FIGURE 5
Cross-sectional morphology of the bottom of a Ni60A + 20% WC + 0.3% graphene composite coating by laser cladding at different laser powers: **(A)** 800 W, **(B)** 1,200 W, **(C)** 1,600 W, **(D)** 2,000 W.

element Ni is also present around the WC particles and in the precipitated phase positions of the rod and block structures. However, the Ni content is lower than in the Ni-based alloy region.

Figure 4 shows the cross-sectional morphology of the middle of a Ni60A + 20% WC + 0.3% graphene composite coating by laser cladding at different laser powers. At a laser power of 800 W, there are fewer WC particles in the middle of the coating and the precipitated phase is dominated by rod and fishbone structures. At a laser power of 1,200 W, the morphology of the middle part of the coating is similar to that at 800 W. At a laser power of 1,600 W, the predominantly flocculent and massive structure of the precipitated phase in the middle of the coating. In detail, there is difference between the top and the middle of the coating at 1,600 W. It is mainly due to the fact that the top part of the coating is in contact with air and dissipates heat at a faster rate. This fact favours nucleation so that the top precipitated phase of the coating appears as a fishbone structure (Ge et al., 2022). When the laser power is 2,000 W, the structure of the precipitated phase in the middle of the coating is similar to that of the 1,600 W condition.

Figure 5 shows the cross-sectional morphology of the bottom of a Ni60A + 20% WC + 0.3% graphene composite coating by laser cladding at different laser powers. When the laser power is 800 W, there is delamination at the interface between the coating and the substrate. This is due to the lower laser power, most of the input energy is absorbed by the coating powder above the substrate. It results in a very small dilution of the cladding layer, resulting in insufficient metallurgical bonding between the cladding layer and the substrate. The phenomenon is very easy to occur when the cladding layer is detached, manifesting itself as the separation of the substrate and the coating. At a laser power of 1,200 W, the metallurgical bonding between the substrate and the coating is metallurgical and the fusion line is relatively flat. At laser power levels of 1,600 W and 2,000 W, the heat input increases further resulting in a deeper melt pool and increased curvature of the fusion line. Large number of columnar crystal structures appear at the bottom of the coating due to slow heat dissipation at the bottom of the coating, a large temperature gradient and grain growth.

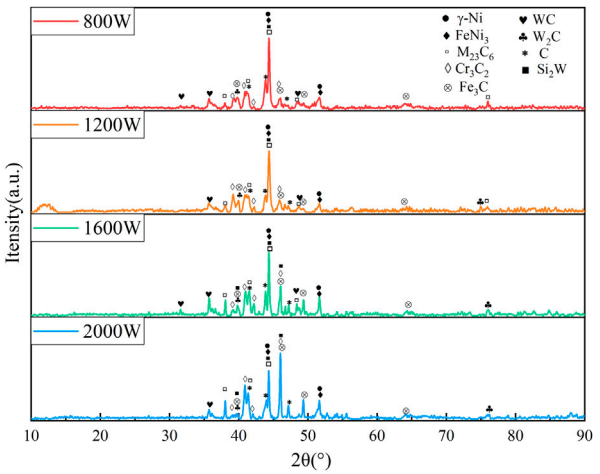

FIGURE 6
XRD results of a composite coating of Ni60A + 20% WC + 0.3% graphene by laser cladding at different laser powers.

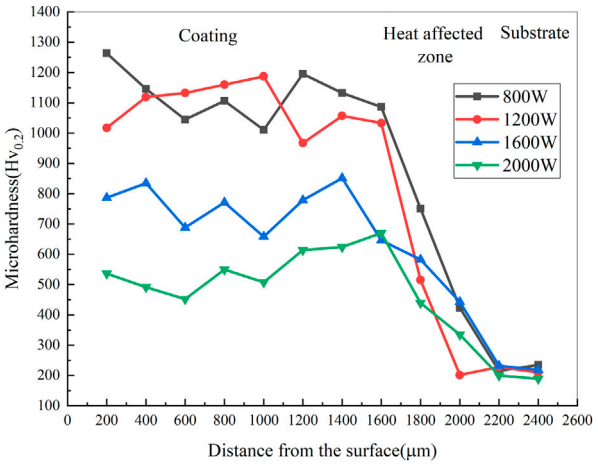

FIGURE 7
Microhardness distribution results of the composite coating of Ni60A + 20% WC + 0.3% graphene by laser cladding at different laser powers.

3.2 XRD analysis

Figure 6 shows the XRD results of the composite coating of Ni60A + 20% WC + 0.3% graphene by laser cladding at different laser powers. The composition of the coating phases at different powers does not differ significantly and consists mainly of γ-Ni, $FeNi_3$, $M_{23}C_6$ (M = Fe, Cr), Cr_3C2, Fe_3C, WC, W_2C, Si_2W and C. However, the intensity of the peaks corresponding to the different species can be judged to be significantly different. When the laser power is 1,600 W, a significant increase in the intensity of the corresponding peaks for $M_{23}C_6$, Cr_3C_2, and Fe_3C can be observed. When the laser power is further increased to 2,000 W, further enhancement of the corresponding peaks of $M_{23}C_6$, Cr_3C_2, and Fe_3C can be observed, and their intensity has surpassed the main peak of the pure Ni60A cladding at 1,200 W power.

3.3 Microhardness analysis

Figure 7 shows the Microhardness distribution results of the composite coating of Ni60A + 20% WC + 0.3% graphene by laser cladding at different laser powers. In Figure 7, the hardness distribution area can be divided into the cladding layer zone, fusion zone, and heat affected zone. The cladding layer zone has the highest hardness, while the fusion zone belongs to the transition zone, and the hardness begins to decrease. It can be seen that the hardness value of the cladding layer zone does not change much, while the hardness of the fusion zone rapidly decreases, indicating that the fusion zone is relatively narrow.

In addition, the average microhardness of the composite coatings at laser powers of 800 W–2,000 W were 1,046 HV, 1031.8 HV, 769.4 HV, and 559 HV respectively. The average hardness of the coating does not change significantly at laser powers of 800 W and 1,200 W. When the laser power exceeds 1,200 W, the hardness of the coating decreases as the laser power increases. When the laser power is 800 W and 1,200 W, there is still a distribution of WC particles on the upper surface of the coating. Although the size of WC particles decreases under 1,200 W conditions, the C and W formed by the decarburization reaction of WC promotes the formation of carbides and W-rich phases in the coating. It plays a role in solid solution strengthening (Chen et al., 2023). When the laser power is further increased, the WC particles on the substrate surface have been completely dissolved. The increased power of the laser causes more energy to enter the substrate resulting in the remelting of the Fe in the substrate and the formation of the Fe_3C phase with the C in the powder. Figure 6 XRD results can be observed that the intensity of the corresponding peaks of the phases of $M_{23}C_6$, Cr_3C_2, and Fe_3C are significantly increased at 1,600 W and 2,000 W. However, the hardness of the above phases is lower than that of WC, so the increase in their content will instead reduce the hardness of the cladding.

4 Conclusion

In this paper, a new type of high hardness coating for improving drill bit stability in unconventional oil and gas development was developed. The present work investigates the microstructure and microhardness of Ni60A + 20% WC + 0.3% graphene composite coatings by laser cladding at different powers, and the following conclusions were obtained:

(1) When the laser power is low, the WC particles do not dissolve sufficiently, the dilution rate of the substrate is low and the metallurgical bond between the coating and the substrate cannot be formed.
(2) Too high laser power leads to a decrease in the microhardness of the coating. When the laser power is 1,200 W, the overall performance is the best.
(3) There is no significant difference in the composition of the coating phases at different power levels, consisting mainly of γ-Ni, $FeNi_3$, $M_{23}C_6$, Cr_3C_2, Fe_3C, WC, W_2C, Si_2W, and C. The percentage of $M_{23}C_6$, Cr_3C_2, and Fe_3C in the coating increased with increasing laser power.

Data availability statement

The original contributions presented in the study are included in the article/Supplementary Material, further inquiries can be directed to the corresponding author.

Author contributions

LX: Conceptualization, Funding acquisition, Investigation, Methodology, Validation, Writing–review and editing. JW: Data curation, Formal Analysis, Writing–original draft.

Funding

The authors declare financial support was received for the research, authorship, and/or publication of this article. This work

was supported by the Open Fund of State Key Laboratory of Shale Oil and Gas Enrichment Mechanisms and Effective Development, and the General Project of Jiangsu Province University Basic Science (NATURAL SCIENCE) Research (grant no. 22KJD430001).

Conflict of interest

Author LX was employed by Sinopec Research Institute of Petroleum Engineering Co. Ltd.

The remaining author declares that the research was conducted in the absence of any commercial or financial relationships that could be construed as a potential conflict of interest.

Publisher's note

References

Chang, W., Xiao, G., Zhang, H., Chen, H., Yi, M., Zhang, J., et al. (2023). Microstructure and properties of graphene reinforced co-based composite coating by laser cladding. *Surf. Coatings Technol.* 453, 129139. doi:10.1016/j.surfcoat.2022.129139

Chen, C., Feng, A., Wei, Y., Wang, Y., Pan, X., and Song, X. (2023). Effects of WC particles on microstructure and wear behavior of laser cladding Ni60 composite coatings. *Opt. Laser Technol.* 163, 109425. doi:10.1016/j.optlastec.2023.109425

Chen, L., Yu, T., Chen, X., Zhao, Y., and Guan, C. (2022). Process optimization, microstructure and microhardness of coaxial laser cladding TiC reinforced Ni-based composite coatings. *Opt. Laser Technol.* 152, 108129. doi:10.1016/j.optlastec.2022.108129

Chiang, K. A., and Chen, Y. (2007). Microstructural characterization and microscopy analysis of laser cladding Stellite12 and tungsten carbide. *J. Mater Process Technol.* 182, 297–302. doi:10.1016/j.jmatprotec.2006.08.007

Dontsov, E. V. (2022). Analysis of a constant height hydraulic fracture driven by a power-law fluid. *Rock Mech. Bull.* 1 (1), 100003. doi:10.1016/j.rockmb.2022.100003

Ge, T., Chen, L., Gu, P., Ren, X., and Chen, X. (2022). Microstructure and corrosion resistance of TiC/Inconel 625 composite coatings by extreme high speed laser cladding. *Opt. Laser Technol.* 150, 107919. doi:10.1016/j.optlastec.2022.107919

Hu, Y., Wang, Z., and Pang, M. (2022b). Effect of WC content on laser cladding Ni-based coating on the surface of stainless steel. *Mater. Today Commun.* 31, 103357. doi:10.1016/j.mtcomm.2022.103357

Hu, Z., Li, Y., Lu, B., Tan, N., Cai, L., and Yong, Q. (2022a). Effect of WC content on microstructure and properties of high-speed laser cladding Ni-based coating. *Opt. Laser Technol.* 155, 108449. doi:10.1016/j.optlastec.2022.108449

Huang, L. K., He, R., Yang, Z. Z., Tan, P., Chen, Z. W., Li, X. G., et al. (2023). Exploring hydraulic fracture behavior in glutenite formation with strong heterogeneity and variable lithology based on DEM simulation. *Eng. Fract. Mech.* 278, 109020. doi:10.1016/j.engfracmech.2022.109020

Jie, G., Yan, S., Kangning, W., Qiang, S., and Canming, W. (2022). Effect of Fe content on microstructure and corrosion resistance of Ni-based alloy formed by laser cladding. *Surf. Coatings Technol.* 446, 128761. doi:10.1016/j.surfcoat.2022.128761

Kendall, O., Abrahams, R., Paradowska, A., Reid, M., Qiu, C., Mutton, P., et al. (2023). Influence of multi-layer laser cladding depositions and rail curvature on residual stress in light rail components. *Eng. Fail. Anal.* 150, 107330. doi:10.1016/j.engfailanal.2023.107330

Li, S., Huang, K., Zhang, Z., Zheng, C., Li, M., Wang, L., et al. (2023). Wear mechanisms and micro-evaluation of WC + TiC particle-reinforced Ni-based composite coatings fabricated by laser cladding. *Mater. Charact.* 197, 112699. doi:10.1016/j.matchar.2023.112699

Li, W., Yang, X., Wang, S., Duan, D., Li, F., Qiao, Y., et al. (2022). The effect of WC content on the bonding strength and mechanical properties of WC/Ni60 coatings of brake disc. *Opt. Laser Technol.* 149, 107822. doi:10.1016/j.optlastec.2021.107822

Liao, Z., Huang, X., Zhang, F., Li, Z., Chen, S., and Shan, Q. (2023). Effect of WC mass fraction on the microstructure and frictional wear properties of WC/Fe matrix composites. *Int. J. Refract. Metals Hard Mater.* 114, 106265. doi:10.1016/j.ijrmhm.2023.106265

Ma, X., Zhang, S., Zhang, X., Liu, J., Jin, J., Cheng, W., et al. (2022). Lithology-controlled stress variations of Longmaxi shale–Example of an appraisal wellbore in the Changning area. *Rock Mech. Bull.* 1 (1), 100002. doi:10.1016/j.rockmb.2022.100002

Meng, L., Sheng, P., and Zeng, X. (2022). Comparative studies on the Ni60 coatings deposited by conventional and induction heating assisted extreme-high-speed laser cladding technology: formability, microstructure and hardness. *J. Mater. Res. Technol.* 16, 1732–1746. doi:10.1016/j.jmrt.2021.12.110

Qunshuang, M., Yajiang, L., Juan, W., and Kun, L. (2016). Microstructure evolution and growth control of ceramic particles in wide-band laser clad Ni60/WC composite coatings. *Mater. Des.* 92, 897–905. doi:10.1016/j.matdes.2015.12.121

Ren, M., Li, R., Zhang, X., Gu, J., and Jiao, C. (2023). Effect of WC particles preparation method on microstructure and properties of laser cladded Ni60-WC coatings. *J. Mater. Res. Technol.* 22, 605–616. doi:10.1016/j.jmrt.2022.11.120

Tan, P., Jin, Y., and Pang, H. W. (2021). Hydraulic fracture vertical propagation behavior in transversely isotropic layered shale formation with transition zone using XFEM-based CZM method. *Eng. Fract. Mech.* 248, 107707. doi:10.1016/j.engfracmech.2021.107707

Tan, P., Pang, H. W., Zhang, R. X., Jin, Y., Zhou, Y. C., Kao, J. W., et al. (2020). Experimental investigation into hydraulic fracture geometry and proppant migration characteristics for southeastern Sichuan deep shale reservoirs. *J. Petroleum Sci. Eng.* 184, 106517. doi:10.1016/j.petrol.2019.106517

Wang, J., Cai, C., Fu, P., Deng, S., and Tang, Z. (2023a). Study on simulation of cement plug-formation interface stripping failure and main influencing factors. *Front. Earth Sci.* 11, 1123620. doi:10.3389/feart.2023.1123620

Wang, J., and Cai, C. (2023b). The failure law of the cement plug-casing interface for direct plugging in the casing of old wells for salt cavern gas storage. *J. Adhesion Sci. Technol.*, 1–18. doi:10.1080/01694243.2023.2240594

Wang, J., Li, J., Liu, G., Liu, S., Ren, M., Luo, K., et al. (2021). Development and application of wellbore heat transfer model considering variable mass flow. *Undergr. Space* 6 (3), 316–328. doi:10.1016/j.undsp.2020.04.001

Wang, Q., Chen, F. Q., Li, Q., Zhang, L., Jin, H., and Zhang, J. W. (2022a). Microstructure and properties of Ni60 alloy coating prepared by electromagnetic compound field assisted laser cladding. *Mater. Chem. Phys.* 291, 126678. doi:10.1016/j.matchemphys.2022.126678

Wang, Q., Li, Q., Zhang, L., Chen, D. X., Jin, H., Li, J. D., et al. (2022b). Microstructure and properties of Ni-WC gradient composite coating prepared by laser cladding. *Ceram. Int.* 48, 7905–7917. doi:10.1016/j.ceramint.2021.11.338

Wu, P., Du, H. M., Chen, X. L., Li, Z. Q., Bai, H. L., and Jiang, E. Y. (2004). Influence of WC particle behavior on the wear resistance properties of Ni–WC composite coatings. *Wear* 257, 142–147. doi:10.1016/j.wear.2003.10.019

Wu, T., Shi, W., Xie, L., Gong, M., Huang, J., Xie, Y., et al. (2022). Effects of re-melting process parameters on the forming quality of the Stellite 6/WC laser cladding layer. *Optik* 269, 169887. doi:10.1016/j.ijleo.2022.169887

Wu, T., Shi, W., Xie, L., Gong, M., Huang, J., Xie, Y., et al. (2023). Study on the effect of Ni60 transition coating on microstructure and mechanical properties of Fe/WC composite coating by laser cladding. *Opt. Laser Technol.* 163, 109387. doi:10.1016/j.optlastec.2023.109387

Xia, J., Yu, Y., Chen, Z., Zhang, S., Guo, F., and Ma, X. (2022). Effect of graphite powder addition on the structure and properties of WC-reinforced Ni-based composite coatings. *Surf. Technol.*, 1–11.

Xu, J.-S., Zhang, X.-C., Xuan, F.-Z., Wang, Z.-D., and Tu, S.-T. (2014). Rolling contact fatigue behavior of laser cladded WC/Ni composite coating. *Surf. Coatings Technol.* 239, 7–15. doi:10.1016/j.surfcoat.2013.11.005

Xu, S., Cai, Q., Li, G., Lu, X., and Zhu, X. (2022). Effect of scanning speed on microstructure and properties of TiC/Ni60 composite coatings on Ti6Al4V alloy by laser cladding. *Opt. Laser Technol.* 154, 108309. doi:10.1016/j.optlastec.2022.108309

Yao, J., Zhang, J., Wu, G., Wang, L., Zhang, Q., and Liu, R. (2018). Microstructure and wear resistance of laser cladded composite coatings prepared from pre-alloyed WC-NiCrMo powder with different laser spots. *Opt. Laser Technol.* 101, 520–530. doi:10.1016/j.optlastec.2017.12.007

Zhang, K., Ju, H., Xing, F., Wang, W., Li, Q., Yu, X., et al. (2023b). Microstructure and properties of composite coatings by laser cladding Inconel 625 and reinforced WC particles on non-magnetic steel. *Opt. Laser Technol.* 163, 109321. doi:10.1016/j.optlastec.2023.109321

Zhang, W., Shang, X., Hu, M., He, X., Yang, B., Dai, K., et al. (2023a). Microstructure and corrosion-wear behaviors for laser cladding repaired martensitic stainless steels using Co-based and Ni-based powders. *Mater. Today Commun.* 35, 106287. doi:10.1016/j.mtcomm.2023.106287